Plasma Ion Emission from High Intensity Picosecond Laser Pulse Interactions with Solid Targets

A. P. Fews,[1] P. A. Norreys,[2] F. N. Beg,[3] A. R. Bell,[3] A. E. Dangor,[3] C. N. Danson,[2] P. Lee,[3] and S. J. Rose[2,4]

[1]*Department of Physics, University of Bristol, Royal Fort, Tyndall Avenue, Bristol, BS8 1TL, United Kingdom*

[2]*Rutherford Appleton Laboratory, Chilton, Didcot, Oxon, OX11 0QX, United Kingdom*

[3]*Imperial College of Science, Technology & Medicine, Prince Consort Road, London, SW7 2AZ, United Kingdom*

[4]*University of Birmingham, Birmingham B15 2TT, United Kingdom*

(Received 3 June 1994)

The fast ion emission from high intensity, picosecond laser plasmas has been measured to give the characteristic ion energy and the amount of laser energy transferred to ions with energies $\geq$100 keV/nucleon as a function of incident intensity. The characteristic ion energy varies from 0.2 to 1.3 MeV over the range 2.0×10^{17}–2.0×10^{18} W cm^{-2}. 10% of the laser energy is transferred into MeV ions at 2.0×10^{18} W cm^{-2}. Calculations of stopping power in high density materials are presented that show that fast ions cannot be ignored in modeling fast ignitor schemes.

PACS numbers: 52.50.Jm

The implementation of chirped pulse amplification (CPA) systems onto high power lasers has made available new intensity regimes that were previously inaccessible in the laboratory. At intensities of 10^{18} W cm^{-2}, the electron oscillatory velocity for 1 μm radiation becomes relativistic and the radiation pressure reaches 300 Mbar. Interesting new physical phenomena have been predicted in this regime, such as ultralarge self-generated magnetic fields, energetic ions in the MeV range, and large amplitude plasma waves [1].

One of the most interesting and exciting suggestions for the use of short pulse, picosecond laser pulses is to use them in conjunction with longer pulses in a compression geometry as a route to achieving fusion conditions with reduced laser drive energy [2]. In inertial confinement fusion schemes, a pellet containing high pressure deuterium-tritium (DT) fuel achieves a large volumetric compression by ensuring a high degree of symmetrical irradiation of the driving laser pulse. Maximum compression is achieved by ensuring that the process takes place isentropically. Significant additional energy is required in the nanosecond drive pulse in order to reach the required temperatures for high gain, generally by creating a hot spark at the center of the fuel by a process of shock wave convergence. Alpha particle heating then ensures that a burn wave propagates through the compressed fuel. The amount of additional energy required to create the hot spark is highly dependent on the degree of spherical convergence. In the fast ignitor scheme [2], superthermal electrons generated by the interactions of short pulses propagate into the high density core and heat a small proportion of the fuel rapidly to ignition conditions before it can disassemble. Fundamental questions need to be addressed in this scheme, such as the behavior of fast particles and their associated energy transport throughout the target.

In this Letter, we present the first observations of the behavior of fast ions created by picosecond laser produced plasmas at 2×10^{18} W cm^{-2}, intensities relevant to fast ignitor studies. One arm of the VULCAN laser delivered up to 30 J of p-polarized, 1053 nm wavelength radiation [3]. The pulse lengths ranged from 1.8 to 4.0 psec. An off-axis parabolic mirror with a focal length of 44 cm focused the radiation onto Mylar disk targets of diameter 270 μm and thickness 36 μm which were placed at 30° to the incident laser light to protect the laser chain from back reflections. The focal spot was measured by an equivalent plane monitor to have dimensions of 15×50 μm. The contrast ratio was measured to be 1:10^6 [4].

The fast ion emission was recorded by CR-39 plastic nuclear track detectors [5]. CR-39 records charged nuclear particles as tracks which are etched into the surface of the detector after the exposure. Each incident ion produces a separate etched track, the dimensions and depth of penetration of which enable the energy and atomic number of the fast ions to be individually determined. The detector is sensitive to ions with energies >100 keV/nucleon. The angular spread of emission was determined by positioning up to 7 detectors around the target; and the total flux of ions was measured simply by counting the number of tracks in the detectors. In all shots, one piece of CR-39 detector was placed in the normal incidence direction at a distance of 55 cm from the target. The CR-39 was covered with an array of 12 Mylar filters that increased in thickness by steps of 2.5 μm and 8 steps of Al of thickness 25 μm. Each step is sensitive to a different energy interval, giving an energy resolution of ~0.1 MeV in the range 0.1–6.0 MeV. At high flux levels where it is not possible to analyze individual particles, the signal under each filter is averaged. In addition, ions with energies in the range 1–10 keV/nucleon were recorded by Faraday cups.

The technique of maximum entropy penumbral imaging was employed to image the ion emission [6]. The technique has previously been employed to measure the shape of implosion cores of inertial confinement fusion targets in three dimensions from alpha particle emission [7]. As the pulse length of the heating beam

is so short, the spatial extent of the plasma is small during the interaction, and the region of fast electron/ion production may be similar in spatial extent to the focal spot dimensions, in contrast to high irradiance interactions with 1.2 nsec pulses [8]. A penumbral imaging camera was formed using a gold aperture of 80 μm diameter located 11.4 mm from the target (a magnification of 15.4). The spatial resolution was calculated from numerical simulations to be ~ 5 μm. The detector had dimensions of 50×50 mm. The camera was at an angle of 35° from the normal in the vertical direction and 37° in the horizontal. Standard pinhole cameras recorded the plasma x-ray emission.

Figure 1(a) shows an example of a reconstructed image of the fast ion emission. In this shot, 30 J of laser energy was incident onto the target in a pulse length of 1.8 psec. The image was formed from the highest energy ions (>3 MeV) to avoid problems with excessive particle fluxes and consequent blurring of the image due to space-charge effects. Ions of the relevant energies in the image were selected from measurement of the individual dimensions of each particle track. A significant nonuniformity in the ion emission can be observed, with a hot spot on one side of the image. A typical equivalent plane image is shown in Fig. 1(b), representing our best estimate of the focal spot distribution. Approximately 70% of the ion emission is contained within an area of 25×75 μm in Fig. 1(a). By comparison, x-ray images from the pinhole cameras show that the heated region around the focal spot was never less than 60 μm in the vertical dimension and increased with increasing laser energy [3]. We believe that the extension of the focal spot dimensions measured in the x-ray images are due to lateral transport of energy away from the heated region.

The ion emission is predominantly from protons. In some cases, emission of carbon ions was also observed. These carbon ions are easily distinguished from protons since they have a much larger energy loss rate in the CR-39, resulting in different track growth characteristics [5]. Although in a few cases the maximum carbon energy was as large as half the maximum proton energy, the flux was much lower, and no more than 10% of the energy was contained in nonhydrogenic ions above 100 keV. We observed that the plasma was confined to a plume emitted along the target normal on the irradiated side of the target, confirming the result of our earlier experiment [3]. The highest energy ions were observed along this normal incidence direction. Similar spectral shapes were observed at all other angles with a slow decrease in maximum energy with increasing angle from the target normal.

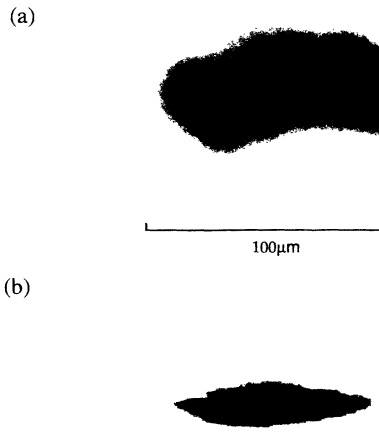

FIG. 1. (a) Reconstructed particle image showing the region of proton emission; (b) equivalent plane image of the far field.

Two typical ion spectra from the forward normal direction are presented in Fig. 2. The ion emission in Fig. 2(a) shows an exponential decreasing profile with increasing energy followed by a sharp cutoff at 4.2 MeV. In this case 32 J in 2.4 psec was incident onto the Mylar target at an incident intensity of 1.9×10^{18} W cm^{-2}. This behavior was typical of two-thirds of the shots. The ion spectrum in Fig. 2(b), however, shows a quite different profile in that the decay with higher energies shows a distinct nonexponential behavior. This was observed in one-third of the extended data set. Here 24 J in 2.6 psec was incident onto the Mylar target at an incident intensity of 1.2×10^{18} W cm^{-2}. A variety of different shapes was observed for the nonexponential profiles, with many of them showing a gentle peak at higher energies as illustrated in Fig. 2(b). The ion

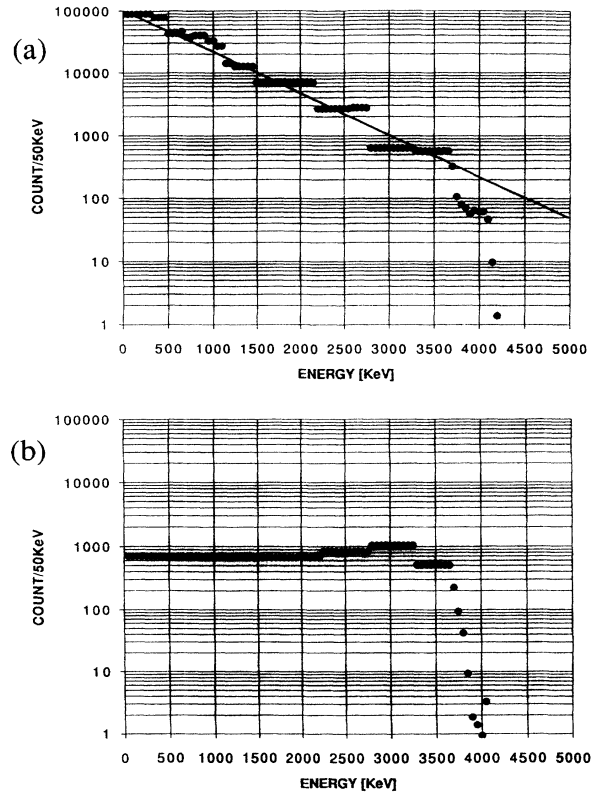

FIG. 2. Normal incidence ion spectra (a) 1.9×10^{18} W cm^{-2} incident intensity showing an exponential profile; (b) 1.2×10^{18} W cm^{-2} incident intensity showing a nonexponential profile.

velocity distribution has been shown to be dependent on scaling parameter $r_s/c\tau$, where r_s is the focal spot radius, c is the sound speed, and τ is the laser pulse length [9]. Hot spots will change the distribution locally and influence the overall ion velocity profile. All of the data show a very sharp cutoff energy: This is a real effect since the particle detection threshold is two orders of magnitude smaller than the lower limit shown in Fig. 2.

The characteristic ion energy can be represented by the mean of the distribution. Figure 3 shows the scaling of the mean energy of the particles in keV plotted against incident intensity. The solid circles and triangles show the mean energy for the exponential and nonexponential spectra, respectively. The two categories of spectra are not resolved from each other within the scatter of the measurements. For interest we have also plotted span of mean ion energies reported by Gitomer *et al.* [10], the limits of which are shown by the two dashed lines, from high irradiance ($I\lambda^2$), nanosecond 10.6 μm laser plasma interactions. Our data are entirely consistent with these high irradiance interaction measurements at longer pulses.

All the ion data show a very sharp cutoff in the ion energy spectra, as illustrated above in Fig. 2. This feature becomes progressively more prominent with higher intensity. The cutoff proton energy recorded in the CR-39 plotted against incident irradiance is also shown in Fig. 3. The open circles and triangles represent the exponential and nonexponential spectral shapes, respectively. Protons with energies up to 5.5 MeV were observed. It can be seen that the cutoff energy is also roughly proportional to the intensity. Wickens, Allen, and Rumsby [11] have shown that, provided there is no electron energy lost to the cold solid target, the electron energy is transferred to the acceleration of the ions with a bi-Maxwellian form: a cold Maxwellian velocity for slow ions and a hot Maxwellian tail of fast ions. Pearlman and Morse observed the fast ion cutoff energy in early laser-plasma experiments [12] and attributed the cutoff to charge separation. This limits the ion velocities by forming a non-neutral electrostatic sheath which truncates the exponential density profile. Kishimoto *et al.* [13] have shown that this cutoff ion energy is proportional to the maximum energy of the hot electrons.

To determine the percentage of laser energy transferred to fast ions, knowledge of the angular distribution of energy is required. Half of the total fast ion emission was confined to a half angle cone of 20°. Measurements in the horizontal and vertical directions indicate that the plasma emission is conically symmetric. Figure 4 shows the percentage of laser energy absorbed as a function of incident intensity. At an intensity of 2.0×10^{18} W cm^{-2}, 10% of the laser energy is transferred to ions with energies >100 keV/nucleon and mean energy of 1.3 MeV.

The scatter in the individual measurements is surprisingly large and has also been observed by Darrow *et al.* [14] and at lower intensities by Meyerhofer *et al.* [15]. The data we present here are for individual laser shots, with 66% of the data lying within a factor of 3 of the best fit line. The percentage of laser energy transferred into fast ions at lower intensities (2×10^{17} W cm^{-2}) is surprisingly small, especially given the absorption data reported by Klem *et al.* [16] who showed that ~20% of the incident laser energy is absorbed at similar intensities to those reported here. This suggests that at higher intensities, nearly all of the absorbed energy is transferred into the emitted fast ions. The measurements shown in Fig. 4 are based on analysis of individual tracks in CR-39 and so are

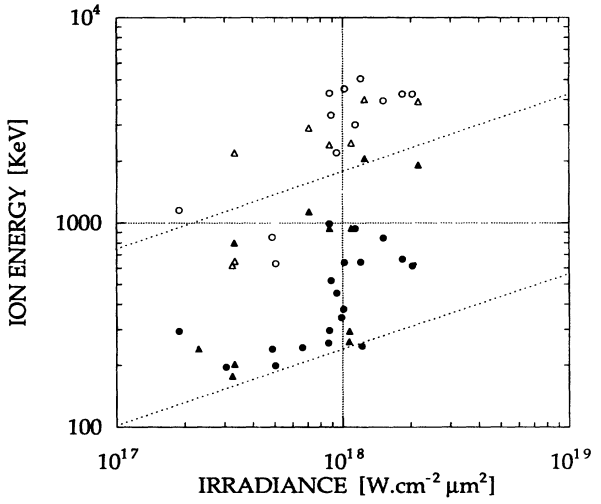

FIG. 3. Characteristic ion energy plotted against irradiance. The solid circles and triangles are the mean ion energies with exponential and nonexponential energy profiles, respectively. The dotted lines represent the limits on the ion energy measurements at longer pulses from Gitomer *et al.* [10]. The open circles and triangles are the cutoff energies for exponential and nonexponential profiles, respectively.

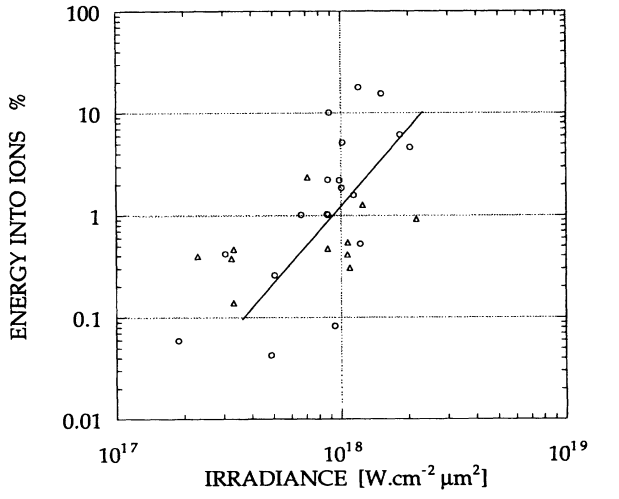

FIG. 4. Percentage of incident energy emitted in the form of fast ions >100 keV as a function of intensity. The circles and triangles represent the exponential and nonexponential spectra, respectively.

accurate measurements of the energy transference to ions above 100 keV for the individual data shots shown. At lower intensities, where the mean ion energy approaches the CR-39 cutoff energy, a significant proportion of the energy can be transferred into other components, although both the proportion transferred and the mean energy fluctuate by an order of magnitude between individual shots. The Faraday cup measurements suggest that ~3% of the laser energy was transferred into ions of 1–10 keV at 2×10^{17} W cm^{-2}, falling to ~0.3% at laser intensities of 2×10^{18} W cm^{-2}, although this is only evident by considering a large number of data shots.

$2\frac{1}{2}$D particle in cell kinetic simulations [1] predict two phenomena: First that the laser bores a hole into the plasma; second that a substantial percentage of the ion emission is directed inwards into the target. These predictions, together with the ion emission behavior presented here, suggest that in the fast ignitor scheme, ion energy deposition may significantly augment the heating by fast electrons. In implosions experiments at Osaka University [17], a deuterated plastic (C_8D_8) with a density and temperature of approximately 600 g cm^{-3} and 300 eV with a fuel $\langle \rho R \rangle \approx 0.1$ gcm^{-2} were measured. Our experiments suggest that the interaction of a short pulse laser with this compressed material would generate fast ions, particularly deuterons. The calculated stopping power with this compressed material in the imploded plastic is shown in Fig. 5. The calculations are based on the Thomas-Fermi model of electronic structure in the plasma and use a local density approximation, including the effect of the free electrons in the plasma being partially degenerate. Figure 5 shows that deuterons generated with energy of a few MeV directed into the target will deposit most of their energy in the plasma. Moreover, there is scope for influencing the energy deposition profile within the plasma by altering the initial energy of the deuteron which, as we have seen, is related to the laser intensity.

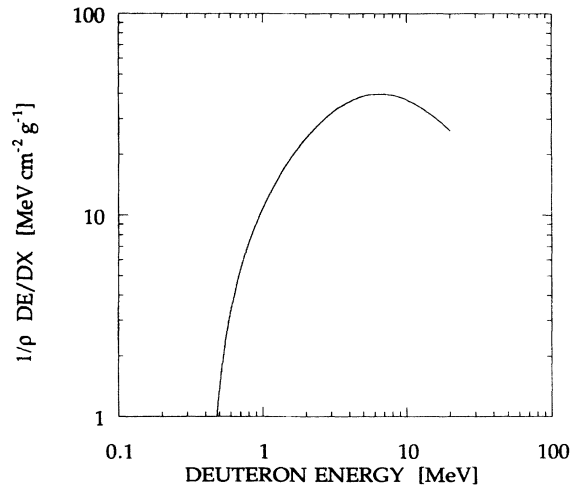

FIG. 5. The calculated stopping power of fast deuteron ions in deuterated plastic at a density of 600 g cm^{-3} and temperature of 300 eV.

In conclusion, we have shown that the characteristic (mean) ion energy varies from 0.2 to 1.3 MeV over the range 1.0×10^{17}–2.0×10^{18} W cm^{-2}. 10% of the laser energy is transferred into ions with energy >100 keV/nucleon, with a mean energy of 1.3 MeV at 2.0×10^{18} W cm^{-2}. We have presented stopping power calculations in high density, partially Fermi degenerate plasmas that suggest that fast ions cannot be ignored in modeling fast ignitor schemes.

[1] W. L. Kruer and S. C. Wilks, Plasma Phys. Controlled Fusion **34**, 2061 (1992).
[2] M. Tabak *et al.*, Phys. Plasmas **1**, 1626 (1994).
[3] A. R. Bell *et al.*, Phys. Rev. E **48**, 2087 (1993).
[4] C. N. Danson, *et al.* Opt. Commun. **103**, 392 (1993).
[5] A. P. Fews and D. L. Henshaw, Nucl. Instrum. Methods Phys. Res. **197**, 512 (1982); A. P. Fews, Nucl. Instrum. Methods Phys. Res., Sect. B **71**, 465 (1992); **72**, 91 (1992).
[6] A. P. Fews, M. J. Lamb, and M. Savage, Opt. Commun. **94**, 259 (1992).
[7] A. P. Fews, M. J. Lamb, and M. Savage, Laser and Particle Beams **12**, 1 (1994).
[8] R. Decoste *et al.*, Phys. Fluids **29**, 328 (1986).
[9] J. Grun, R. Stellingwerf, and B. H. Ripin, Phys. Fluids **29**, 3390 (1986).
[10] S. J. Gitomer *et al.*, Phys. Fluids **29**, 2679 (1986).
[11] L. M. Wickens, J. E. Allen, and P. T. Rumsby, Phys. Rev. Lett. **41**, 243 (1978).
[12] J. S. Pearlman and R. L. Morse, Phys. Rev. Lett. **40**, 1652 (1978).
[13] Y. Kishimoto, K. Mima, T. Watanabe, and K. Nichikawa, Phys. Fluids **26**, 2316 (1983).
[14] C. Darrow, S. Lane, D. Klem, and M. D. Perry, in *Short Pulse High-Intensity Lasers and Applications II,* edited by H. A. Baldis (Proceedings of the International Society for Optical Engineering) **1860**, 46–50 (1993).
[15] D. D. Meyerhofer *et al.*, Phys. Fluids B **5**, 2584 (1993).
[16] D. Klem, C. Darrow, S. Lane, and M. D. Perry, in *Short Pulse High Intensity Lasers and Applications II,* edited by H. A. Baldis (Proceedings of the International Society for Optical Engineering) **1860**, 98–101 (1993).
[17] H. Azechi *et al.*, Lasers and Particles Beams **9**, 193 (1991).

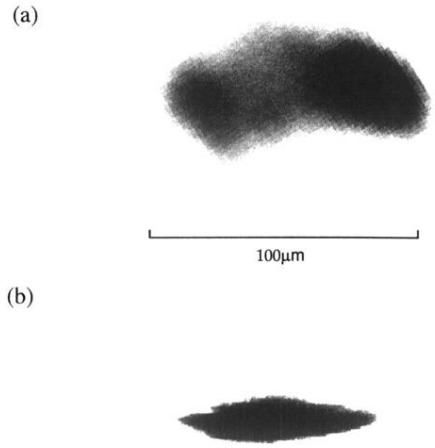

FIG. 1. (a) Reconstructed particle image showing the region of proton emission; (b) equivalent plane image of the far field.